

# DPA-1: Pretraining of Attention-based Deep Potential Model for Molecular Simulation

Duo Zhang<sup>a,b,c</sup>, Hangrui Bi<sup>a,c</sup>, Fu-Zhi Dai<sup>c</sup>, Wanrun Jiang<sup>c</sup>,  
Linfeng Zhang<sup>a,c,\*</sup>, and Han Wang<sup>d,e,\*</sup>

<sup>a</sup>DP Technology, Beijing 100080, P. R. China;

<sup>b</sup>Academy for Advanced Interdisciplinary Studies, Peking University,  
Beijing 100871, P. R. China;

<sup>c</sup>AI for Science Institute, Beijing 100080, P. R. China;

<sup>d</sup>Laboratory of Computational Physics, Institute of Applied Physics and  
Computational Mathematics, Beijing 100094, P. R. China;

<sup>e</sup>HEDPS, CAPT, College of Engineering, Peking University, Beijing 100871, P. R. China.

\*linfeng.zhang.zlf@gmail.com; wang\_han@iapcm.ac.cn

## Abstract

Machine learning assisted modeling of the inter-atomic potential energy surface (PES) is revolutionizing the field of molecular simulation. With the accumulation of high-quality electronic structure data, a model that can be pretrained on all available data and finetuned on downstream tasks with a small additional effort would bring the field to a new stage. Here we propose DPA-1, a Deep Potential model with a novel attention mechanism, which is highly effective for representing the conformation and chemical spaces of atomic systems and learning the PES. We tested DPA-1 on a number of systems and observed superior performance compared with existing benchmarks. When pretrained on large-scale datasets containing 56 elements, DPA-1 can be successfully applied to various downstream tasks with a great improvement of sample efficiency. Surprisingly, for different elements, the learned type embedding parameters form a *spiral* in the latent space and have a natural correspondence with their positions on the periodic table, showing interesting interpretability of the pretrained DPA-1 model.

## 1 Introduction

Reliably representing the inter-atomic potential energy surface (PES) is core to the study of properties of molecules and materials in computational physics, chemistry, materials science, biology, etc. While electronic structure methods typically give accurate and transferable PES, they are prohibitively expensive for scaling to systems of more than thousands of atoms. On the other hand, empirical force fields are much more efficient, but are inherently limited by their accuracy in many applications. By properly integrating machine learning (ML) methodologies and physical requirements like extensiveness and symmetries, various methods have emerged to address the accuracy *v.s.* efficiency dilemma in the realm of PES modeling [1–11]. Arguably, a new paradigm is forming: electronic structure methods are no longer used to generate the driving forces during molecular dynamics simulations but are used to generate data for training their alternatives, ML-based PES models.

Despite remarkable achievements of ML-based PES models [12–14], challenges still remain. For a domain expert who would like to apply such methodologies in their applications, a natural first question is on the efforts needed for obtaining a reliable PES model: Are there ready-to-use PES

models? If not, what would be the amount of training data and time cost required? Can we take advantage of the ever-increasing publicly-available training data?

To address these issues, there have been several efforts. On one hand, general-purpose models for various systems, such as silicon [15], phosphorus [16], water [17], metals and alloys [18–22], etc., have been developed and are directly applicable to relevant studies. However, the range of applicability of such models is typically limited to small conformation or chemical space. For example, for alloys, the majority of general-purpose ML models are developed for systems with at most two element types. On the other hand, several efficient data generation protocols have been developed [23–26], of which a representative is DP-GEN [25, 26], a concurrent learning procedure that iteratively explores the configuration space using models trained with existing data, and then labels only those configurations with high uncertainty level. Even with these protocols, the computational effort needed for complicated systems is still prohibitive. For example, to train a fairly general-purpose model for the AlMgCu alloy system, 100k density functional theory (DFT) [27, 28] calculations were ultimately performed, resulting in the cost of ten million CPU core hours [18].

With the accumulation of high-quality electronic structure data covering almost all the elements on the periodic table, it is becoming possible to systematically develop pretraining schemes, which have been widely adopted in areas like computer vision (CV) [29, 30] and natural language processing (NLP) [31, 32]. In these schemes, one first trains a unified model on large-scale datasets and then finetunes it for downstream tasks, expecting that a good representation can be learned in the first stage, and the amount of supervised data needed for the second stage will be significantly reduced. Unfortunately, most ML-based PES models are premature for such schemes at scale. Taking the widely used two versions of Deep Potential models [6, 7] as examples, the ML parameters are element-type-dependent, making it highly inefficient when the training data containing many elements. Despite some recent attempts on developing “universal” PES models [33, 34], their performance of fine-tuning on downstream tasks and large-scale applications is yet to be seen.

In this article, we propose DPA-1, a Deep Potential model with a novel attention mechanism [35, 30], which is highly effective for learning the inter-atomic interactions and, upon pretraining, can significantly reduce the additional efforts for downstream tasks. We tested DPA-1 on various systems and observed superior performance compared with existing benchmarks. Then we took AlMgCu alloy systems [18] as an example, showing that after pretraining with single-element and binary samples, DPA-1 can save around 90% ternary samples compared with the DeepPot-SE model [7]. Finally, we pretrained DPA-1 using the Open Catalyst 2020 Dataset (OC20) [36], which consists of 56 elements, and successfully applied it to various downstream tasks. We checked the interpretability of the pretrained model by looking into the learned embedding parameters for different element types, finding that the 56 elements are arranged on a *spiral* in the latent space, which has a natural correspondence with their physical properties on the periodic table. Above all, we believe that DPA-1 and the pretraining scheme will bring the field of molecular simulation to a new stage.

We notice that there have been efforts on applying the pretraining scheme to organic molecules [37, 38] and considering tasks beyond representing the PES [39–41]. Here we focus more on extended systems and target at a much larger element space.

## 2 Method

Consider a system of  $N$  atoms, the elemental types are  $\mathcal{A} = \{\alpha_1, \alpha_2, \dots, \alpha_i, \dots, \alpha_N\}$ , and the atomic coordinates are  $\mathcal{R} = \{\mathbf{r}_1, \mathbf{r}_2, \dots, \mathbf{r}_i, \dots, \mathbf{r}_N\}$ , with  $\mathbf{r}_i$  being the three Cartesian coordinates of atom  $i$ . The PES of the system is denoted by  $E$ , a function of elemental types and coordinates, i.e.  $E = E(\mathcal{A}, \mathcal{R})$ . For each atom  $i$ , consider its neighbors  $\{j | j \in \mathcal{N}_{r_c}(i)\}$ , where  $\mathcal{N}_{r_c}(i)$  denotes the set of atom indices  $j$  such that  $r_{ji} < r_c$ , with  $r_{ji}$  being the Euclidean distance between atoms  $i$  and  $j$ .  $E$  is represented as the summation of atomic energies  $\{e_1, e_2, \dots, e_i, \dots, e_N\}$ , where the atomic energy  $e_i$  only depends on the information of  $\mathcal{N}_{r_c}(i)$ . We define  $N_i = |\mathcal{N}_{r_c}(i)|$ , the cardinality of the set  $\mathcal{N}_{r_c}(i)$ . We use  $\mathcal{A}^i$  to denote element types in  $\mathcal{N}_{r_c}(i)$ , and  $\mathcal{R}^i \in \mathbb{R}^{N_i \times 3}$  their corresponding coordinates relative to  $i$ . The atomic energy  $e_i$  is thus a function of  $\mathcal{A}^i$  and  $\mathcal{R}^i$ . The atomic force on atom  $i$ ,  $\mathcal{F}_i$ , is defined as the negative gradient of the total energy with respect to  $i$ ’s coordinate:

$$\mathcal{F}_i = -\nabla_{\mathbf{r}_i} E. \quad (1)$$

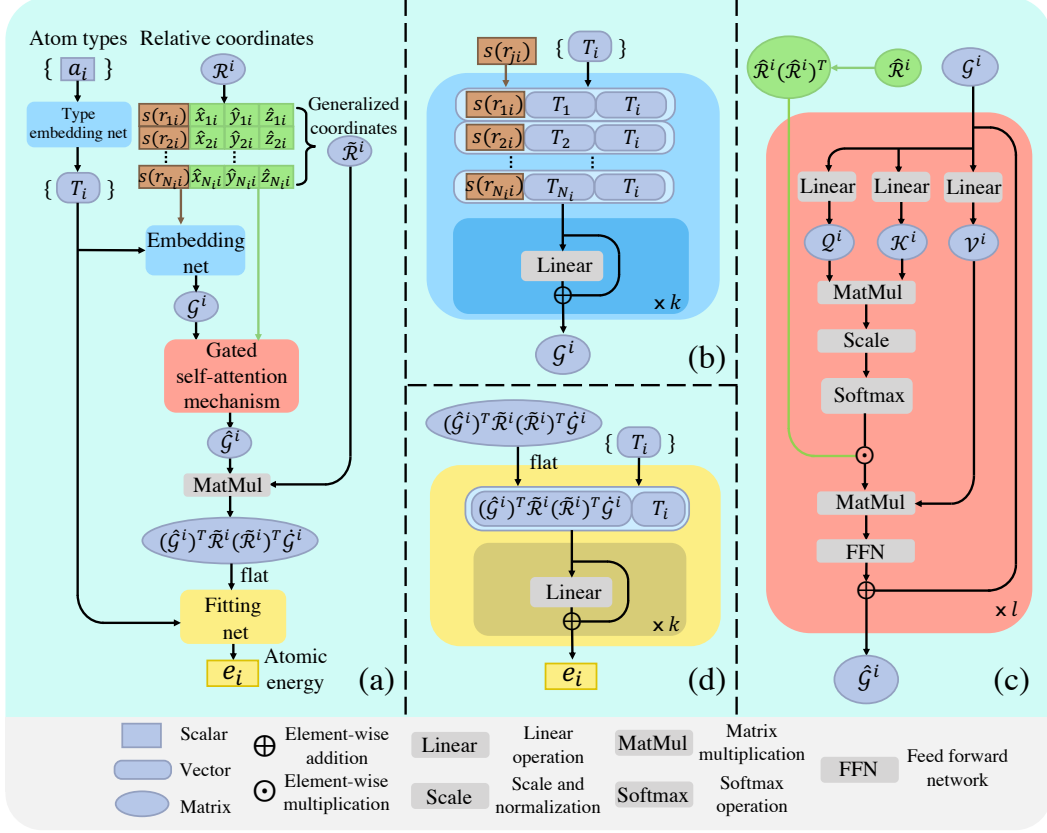


Figure 1: Schematic illustration of DPA-1. (a) Flowchart from  $\mathcal{A}^i$  and  $\mathcal{R}^i$  to the atomic energy  $e_i$ . (b) Structure of the Embedding net, which maps  $s(r_{ji})$  and  $T_i$ , through multiple residual layers, to  $\mathcal{G}^i$ . (c) Self-attention mechanism on  $\mathcal{G}^i$  through a standard scale-dot procedure gated by the angular information  $\hat{\mathcal{R}}^i(\hat{\mathcal{R}}^i)^T$ . (d) Fitting net structures, similar to Embedding net, from the descriptors  $\mathcal{D}^i$  and  $T_i$  to final atomic energy  $e_i$ .

We refer to Ref. [7] for a detailed discussion on several requirements on PES modeling. In particular, the PES has to be invariant under translation, rotation, and permutation of the indices of atoms with the same element types.

The details of the model architecture are introduced below. We refer to Fig. 1 for the overall pipeline to predict the atomic energy  $e_i$ : from the embedded neighboring environment, through the self-attention scheme, to the symmetry-preserving descriptors, and finally to the fitting network.

## 2.1 Local embedding matrix with type information

We obtain the local embedding matrix with the following three steps. First,  $\mathcal{R}^i$  is mapped to the generalized coordinates  $\tilde{\mathcal{R}}^i \in \mathbb{R}^{N_i \times 4}$ . In this mapping, each row of  $\mathcal{R}^i$ ,  $\{x_{ji}, y_{ji}, z_{ji}\}$ , is transformed into a row of  $\tilde{\mathcal{R}}^i$ :

$$\{x_{ji}, y_{ji}, z_{ji}\} \mapsto \{s(r_{ji}), \hat{x}_{ji}, \hat{y}_{ji}, \hat{z}_{ji}\}, \quad (2)$$

where  $\{x_{ji}, y_{ji}, z_{ji}\}$  denotes the Cartesian coordinates of  $\mathbf{r}_{ji} = \mathbf{r}_j - \mathbf{r}_i$ ,  $\hat{x}_{ji} = \frac{s(r_{ji})x_{ji}}{r_{ji}}$ ,  $\hat{y}_{ji} = \frac{s(r_{ji})y_{ji}}{r_{ji}}$ ,  $\hat{z}_{ji} = \frac{s(r_{ji})z_{ji}}{r_{ji}}$ , and  $s(r_{ji}) : \mathbb{R} \mapsto \mathbb{R}$  is a continuous and differentiable scalar weighting function applied to each component, defined as:

$$s(r_{ji}) = \begin{cases} \frac{1}{r_{ji}} & r_{ji} < r_{cs} \\ \frac{1}{r_{ji}} [u^3 (-6u^2 + 15u - 10) + 1] & r_{cs} \leq r_{ji} < r_c, \quad u = \frac{r_{ji} - r_{cs}}{r_c - r_{cs}} \\ 0 & r_c \leq r_{ji} \end{cases} \quad (3)$$

Here  $r_{cs}$  is a smooth cutoff parameter that allows the components in  $\tilde{\mathcal{R}}^i$  to smoothly go to zero at the boundary of the local region defined by  $r_c$ .

Second, we add the atomic type embedding as supplemental information. For atom  $i$ , the type embedding map  $T_i$  is defined as:

$$T_i = \phi_T(\alpha_i), \quad (4)$$

where  $\alpha_i$  is the atomic type of atom  $i$  and  $\phi_T$  is a one-hot-like embedding network mapping from  $\alpha_i$  to a length-fixed vector.

Then, given both  $\tilde{\mathcal{R}}^i$  and type embeddings  $\{T_i\} \cup \{T_j | j \in \mathcal{N}_{r_c}(i)\}$ , we define the local embedding matrix  $\mathcal{G}^i \in \mathbb{R}^{N_i \times M_1}$ :

$$(\mathcal{G}^i)_j = G(s(r_{ji}), T_i, T_j), \quad (5)$$

where  $G$  is a neural network mapping from scalar weight  $s(r_{ji})$  and type embeddings of both center and neighbor atoms, through multiple hidden layers, to  $M_1$  outputs. Here we simply feed the concatenated inputs into  $G$  at once, as shown in Fig. 1(b).

## 2.2 Attention method for building up trainable descriptors

The attention mechanism has achieved great success and played an increasingly important role in CV [42] and NLP [43]. It has become an excellent tool for modeling the importance or relevance of visual regions or text tokens, thus is potentially appropriate to reweight the interactions among neighbor atoms according to both distance and angular information.

In DPA-1, we follow the standard self-attention mechanism and obtain the queries  $\mathcal{Q}^{i,l} \in \mathbb{R}^{N_i \times d_k}$ , keys  $\mathcal{K}^{i,l} \in \mathbb{R}^{N_i \times d_k}$ , and values  $\mathcal{V}^{i,l} \in \mathbb{R}^{N_i \times d_v}$ :

$$(\mathcal{Q}^{i,l})_j = Q_l((\mathcal{G}^{i,l-1})_j), (\mathcal{K}^{i,l})_j = K_l((\mathcal{G}^{i,l-1})_j), (\mathcal{V}^{i,l})_j = V_l((\mathcal{G}^{i,l-1})_j), \quad (6)$$

where  $Q_l, K_l, V_l$  represent three linear transformations which output the queries and keys of dimension  $d_k$  and values of dimension  $d_v$ , and  $l$  is the index of attention layer. Here we take  $\mathcal{G}^{i,0} = \mathcal{G}^i$ .

Then we adopt the scaled dot-product attention method[35] to mix the neighbor features after calculating the attention weights:

$$A(\mathcal{Q}^{i,l}, \mathcal{K}^{i,l}, \mathcal{V}^{i,l}, \mathcal{R}^{i,l}) = \varphi(\mathcal{Q}^{i,l}, \mathcal{K}^{i,l}, \mathcal{R}^{i,l}) \mathcal{V}^{i,l}, \quad (7)$$

where  $\varphi(\mathcal{Q}^{i,l}, \mathcal{K}^{i,l}, \mathcal{R}^{i,l}) \in \mathbb{R}^{N_i \times N_i}$  is attention weights. In the original attention method, one typically has  $\varphi(\mathcal{Q}^{i,l}, \mathcal{K}^{i,l}) = \text{softmax}\left(\frac{\mathcal{Q}^{i,l}(\mathcal{K}^{i,l})^T}{\sqrt{d_k}}\right)$ , with  $\sqrt{d_k}$  being the normalization temperature. This is slightly modified to better incorporate the angular information:

$$\varphi(\mathcal{Q}^{i,l}, \mathcal{K}^{i,l}, \mathcal{R}^{i,l}) = \text{softmax}\left(\frac{\mathcal{Q}^{i,l}(\mathcal{K}^{i,l})^T}{\sqrt{d_k}}\right) \odot \hat{\mathcal{R}}^i(\hat{\mathcal{R}}^i)^T, \quad (8)$$

where  $\hat{\mathcal{R}}^i = \frac{\mathcal{R}^i}{\|\mathcal{R}^i\|_2} \in \mathbb{R}^{N_i \times 3}$  denotes normalized relative coordinates and  $\odot$  means element-wise multiplication. Intuitively, in the neighborhood of center atom  $i$ , neighbor atom  $k$  may be highly correlated with  $j$  when both the relative distance attention  $(\mathcal{Q}^{i,l})_j(\mathcal{K}^{i,l})_k^T$  and normalized product of relative coordinates  $\frac{\mathbf{r}_{ji}(\mathbf{r}_{ki})^T}{r_{ji}r_{ki}}$  have high scores.

Then we add layer normalization in a residual way to finally obtain the self-attended local embedding matrix  $\hat{\mathcal{G}}^i$  in one such attention layer:

$$\mathcal{G}^{i,l} = \mathcal{G}^{i,l-1} + \text{LayerNorm}(A(\mathcal{Q}^{i,l}, \mathcal{K}^{i,l}, \mathcal{V}^{i,l}, \mathcal{R}^{i,l})). \quad (9)$$

We also tried other attention related tricks such as pre-layer normalization, multi-head attention, etc., which brought little improvement. In practice, as shown in Fig. 1(c), we repeated this procedure by  $l(l \geq 2)$  times for a more complete representation.

Next, we define the encoded feature matrix  $\mathcal{D}^i \in \mathbb{R}^{M_1 \times M_2}$  of atom  $i$ :

$$\mathcal{D}^i = \left(\hat{\mathcal{G}}^i\right)^T \tilde{\mathcal{R}}^i \left(\tilde{\mathcal{R}}^i\right)^T \dot{\mathcal{G}}^i, \quad (10)$$

where  $\dot{\mathcal{G}}^i$  stands for a sub-matrix of  $\hat{\mathcal{G}}^i$ , which takes the first  $M_2 (< M_1)$  columns of  $\hat{\mathcal{G}}^i$ . Here the feature matrix  $\mathcal{D}^i$ , i.e. the descriptor, preserves all the invariance mentioned above, of which the proof can be found in Ref. [7]. We then pass the reshaped  $\mathcal{D}^i$ , concatenated with the type embedding parameters of the center atom, through the multi-layer fitting network:

$$e_i = e(\mathcal{D}^i, T_i). \quad (11)$$

The total energy of the system is then given as the summation of  $e_i$ , and the atomic force  $\mathcal{F}_i$  can be further computed via Eq.1.

### 2.3 Model (pre-)training and finetuning

For model training or pretraining, we adopted the Adam stochastic gradient descent method [44] on all the trainable parameters  $w$  inside the model to minimize the loss:

$$\mathcal{L}_w(E^w, \mathcal{F}^w) = \frac{1}{|\mathcal{B}|} \sum_{t \in \mathcal{B}} \left( p_e |E_t - E_t^w|^2 + p_f |\mathcal{F}_t - \mathcal{F}_t^w|^2 \right). \quad (12)$$

Here  $\mathcal{B}$  represents a minibatch,  $|\mathcal{B}|$  is the batch size,  $t$  denotes the index of the training sample.  $E^w, \mathcal{F}^w$  denote the model outputs and  $E, \mathcal{F}$  are the corresponding DFT results. We also adopted a scheduler to tune the prefactors  $p_e$  and  $p_f$  during the training process to make a better balance between energy and force labels. Virial errors, which are omitted here, can be added to the loss for training if available.

To finetune the pretrained model with a new dataset, we first change the energy bias in the last layer of the pretrained model with the new statistical results of the new dataset, and then we fix part of the parameters in the pretrained model and train the remaining. For the following experiments, we obtained the best performance when only the type embedding parameters are fixed.

## 3 Experiments

We conducted a number of experiments to evaluate the performance of DPA-1. First, we trained it from scratch against various systems and compared it with several schemes. Then, we used an AlMgCu dataset to test its ability to transfer to ternary systems upon pretraining with single-element and binary data. Finally, we pretrained DPA-1 using the OC2M subset in OC20 dataset [36] and applied it to various downstream tasks. To illustrate the effectiveness of the type-embedding and attention schemes, we compared against DeepPot-SE model [7] in all the experiments. In the following, we shall introduce first the datasets we used, and then the experiments we conducted.

### 3.1 Datasets

**Simple bulk systems [6].** This small dataset contains two types of systems. The first type includes general systems, such as relatively easy Cu, Ge, Si, Al<sub>2</sub>O<sub>3</sub> with one single solid phase, and more challenging systems like C<sub>5</sub>H<sub>5</sub>N (pyridine) and TiO<sub>2</sub> with two and three phases, respectively. The second type of systems contains a grand-canonical-like system of supported Pt clusters on a MoS<sub>2</sub> slab and a CoCrFeMnNi high entropy alloy (HEA) system.

Table 1: Prediction RMSE of energies (meV/atom) and atomic forces (meV/Å) given by DPA-1 (OC2M-pretrained), DPA-1 (from scratch), EANN, and DeepPot-SE. DPA-1 (OC2M-pretrained) means that the results were obtained by funetuning a DPA-1 model pretrained using the OC2M dataset. For training DPA-1, EANN, and DeepPot-SE, 10%, 15~20%, and 90% randomly sampled data points are used, respectively. Bold numbers correspond to lowest values.

Systems	Sub-systems	Energy (meV/atom) and Force (meV/Å) RMSE							
		DPA-1 (OC2M -pretrained)		DPA-1		EANN		DeepPot-SE	
		Energy	Force	Energy	Force	Energy	Force	Energy	Force
Cu	FCC solid	<b>0.12</b>	<b>86</b>	0.14	88	0.16	89	0.18	90
Ge	diamond solid	0.09	<b>21</b>	0.10	24	<b>0.07</b>	31	0.35	38
Si	diamond solid	0.09	<b>23</b>	0.11	25	<b>0.08</b>	28	0.24	36
Al <sub>2</sub> O <sub>3</sub>	Trigonal solid	<b>0.08</b>	<b>40</b>	0.08	41	0.11	51	0.23	49
C <sub>5</sub> H <sub>5</sub> N	Pyridine-I	<b>0.17</b>	<b>21</b>	0.21	23	<b>0.17</b>	41	0.38	25
	Pyridine-II	<b>0.24</b>	<b>29</b>	0.26	32	0.35	49	0.65	39
TiO <sub>2</sub>	Rutile	0.56	<b>109</b>	0.62	112	<b>0.51</b>	133	0.96	137
	Anatase	<b>0.87</b>	<b>144</b>	0.91	151	1.03	183	1.78	181
	Brookite	<b>0.50</b>	<b>88</b>	0.52	91	0.55	96	0.59	94
MoS <sub>2</sub> +Pt	MoS <sub>2</sub> slab	<b>0.14</b>	<b>11</b>	0.17	12	0.26	19	5.26	23
	bulk Pt	<b>0.25</b>	<b>41</b>	0.26	43	0.38	64	2.00	84
	Pt surface	<b>0.59</b>	<b>45</b>	0.68	<b>45</b>	3.8	86	6.77	105
	Pt cluster	<b>1.21</b>	<b>41</b>	1.33	<b>41</b>	9.7	152	30.6	201
	Pt on MoS <sub>2</sub>	4.43	<b>86</b>	5.02	88	<b>1.33</b>	91	2.62	94
CoCrFe	rand.occ.I	<b>1.31</b>	<b>367</b>	1.43	387	2.3	410	1.68	394
MnNi	rand.occ.II	<b>1.74</b>	<b>381</b>	1.93	389	3.3	415	5.29	410

**AlMgCu alloy systems [18].** This dataset is generated using DP-GEN [26], a concurrent learning scheme. After exploring 2.73 billion alloy configurations (derived from  $\sim 2000$  bulk and surface systems), only a small portion ( $\sim 100k$  configurations) of them are labeled then compose the compact dataset. The exploration runs in the whole concentration space, i.e.,  $\text{Al}_x\text{Cu}_y\text{Mg}_z$  with  $0 \leq x, y, z \leq 1$ ,  $x + y + z = 1$ , and  $x, y, z$  take discrete values permitted by the finite-size simulation boxes. We can divide the systems into *single*, *binary* and *ternary* subsets, in name of the number of non-zero  $x, y, z$ . The configuration space covers a temperature range around 50.0 K to 2579.8 K and a pressure range around 1 bar to 50000 bar.

**Solid-state electrolyte (SSE) systems [45].** These systems contain  $\text{Li}_{10}\text{XP}_2\text{S}_{12}$ -type SSE materials, where X represents single or combination of Ge/Si/Sn, and can be divided into three main parts: *init*, *mix* and *single*. The *init* part comes from standard DP-GEN scheme starting from 590 structures that are generated via slightly perturbing DFT-relaxed crystal structures  $\text{Li}_{10}\text{Ge}(\text{PS}_6)_2$ ,  $\text{Li}_{10}\text{SiP}_2\text{S}_{12}$  and  $\text{Li}_{10}\text{SnP}_2\text{S}_{12}$  from Materials Project [46]. The exploration covers both ordered structures relaxed by DFT (i.e. structures downloaded from the Materials Project database, in which the position of Ge/Si/Sn/P atoms are fixed) and disordered structures whose 4d sites are randomly occupied by Ge/Si/Sn/P. Based on the *init* part, the *mix* part contains further exploration in binary and ternary mixture of Ge/Si/Sn, while the *single* part covers only single X in Ge/Si/Sn with other changes in lattice and ratio of Li.

**HEA systems.** The High Entropy Alloy HEA dataset includes bulk TaNbWMoVAl alloy systems of various configurations and compositions. We employ DP-GEN to explore the composition space, starting from  $\text{Ta}_3\text{Nb}_3\text{W}_3\text{Mo}_3\text{V}_3\text{Al}_1$ , a 16-atom unit cell containing the former 5 elements as main components and Al as an additive. The dataset is divided into two subsets: *interior* and *exterior*. The *interior* (higher entropy) subset includes composition variations near the starting point. It covers six-component, quinary, quaternary and ternary alloys. The *exterior* (lower entropy) subset includes systems that are close to the corners and edges of the composition space. It includes systems where

Table 2: Validation RMSE of DPA-1 and DeepPot-SE on energy (meV/atom) and atomic forces (meV/Å) with different settings of the training/validation sets (See Sec. 3.1 for details). Bold numbers correspond to lower values.

Systems	Training	Validation	Validation RMSE			
			DPA-1		DeepPot-SE	
			Energy	Force	Energy	Force
AlMgCu	single + binary	ternary	<b>6.99</b>	<b>58</b>	65.1	92
	all (single + binary + ternary)	ternary	<b>2.26</b>	<b>35</b>	3.16	42
	all	all	<b>2.74</b>	<b>38</b>	3.67	45
SSE	init + single	mix	<b>0.56</b>	<b>60</b>	0.72	76
	init + mix	single	<b>3.72</b>	<b>69</b>	3.76	82
	all (init + single + mix)	all	<b>1.41</b>	<b>68</b>	2.92	85
HEA	interior	exterior	<b>4.54</b>	<b>86</b>	292	369
	exterior	interior	<b>2.88</b>	<b>62</b>	61.2	276
	all (interior + exterior)	all	<b>4.34</b>	<b>60</b>	27.2	108

one or two elements dominate, binary alloys and simple substance systems. For both subsets, the temperature range is around 50.0 K to 388.1 K and the pressure range is around 1 bar to 50000 bar.

**OC20 [36].** OC20 consists of single adsorbates (small molecules) physically binding to the surfaces of catalysts covering periodic bulk materials with 56 elements. Both the chemical diversity and system size are much more complex than other benchmark datasets, such as MD17 [47], ANI-1x [24] or QM9 [48]. OC2M is a subset including 2 million data points (energies and forces) randomly sampled from OC20, which is still challenging for model training and decent for pretraining. Johannes et al. recently provided several baselines on OC2M, taking months to converge[34].

### 3.2 Accuracy on various datasets, trained from scratch

As shown in Table 1, we trained DPA-1 from scratch on simple bulk systems and compared with the embedded atom neural network potential (EANN) [10] and DeepPot-SE. For training DPA-1 and EANN, only 10% and 15~20% randomly selected data points are used respectively, while DeepPot-SE used 90%. The results show that, even with less training samples and trained from scratch, DPA-1 still mostly outperforms the other methodologies, especially in terms of force prediction accuracy.

To further test the model’s ability to transfer among different compositions, we designed several challenging tasks. For AlMgCu, SSE, and HEA systems, we divided them into subsets with different compositions for training and validation (See Sec. 3.1 for details). The results of DPA-1 and DeepPot-SE are shown in Table 2. With the training loss nearly the same (omitted in the table), DPA-1 drastically outperforms DeepPot-SE in validation accuracy. For example, for AlMgCu systems, when trained only on single-element and binary samples, the validation RMSE of DPA-1 on ternary samples can outperform DeepPot-SE by one order of magnitude (6.99 versus 65.1 meV/atom). This suggests that the DPA-1 model might have learned the latent interactions of ternary pairs Al-Mg-Cu from binary pairs Al-Mg, Al-Cu, Mg-Cu, and single-element interactions, possibly thanks to the type-embedding scheme and attention mechanism.

To test the performance of DPA-1 in terms of predicting more physical quantities, we used it to calculate the elastic moduli of AlMgCu systems, which requires accurately capturing the second-order information. As shown in Fig. A.1, satisfactory results are obtained.

### 3.3 Sample efficiency of pretrained models

As shown in Fig. 2, we use the learning curves to illustrate in terms of the amount of additional training data saved for downstream tasks thanks to model pretraining. In all the experiments, the learning curves were generated by an active learning procedure, in which a pool of data labeled by energy and force is prepared and three steps are repeated iteratively: using samples in the training pool to train the model; testing the model using the remaining samples; selecting 50 samples with the largest prediction errors on per-atom energies and adding them to the training pool. We use the term sample efficiency to denote the amount of training samples required by a model to achieve a given accuracy level for a certain task.

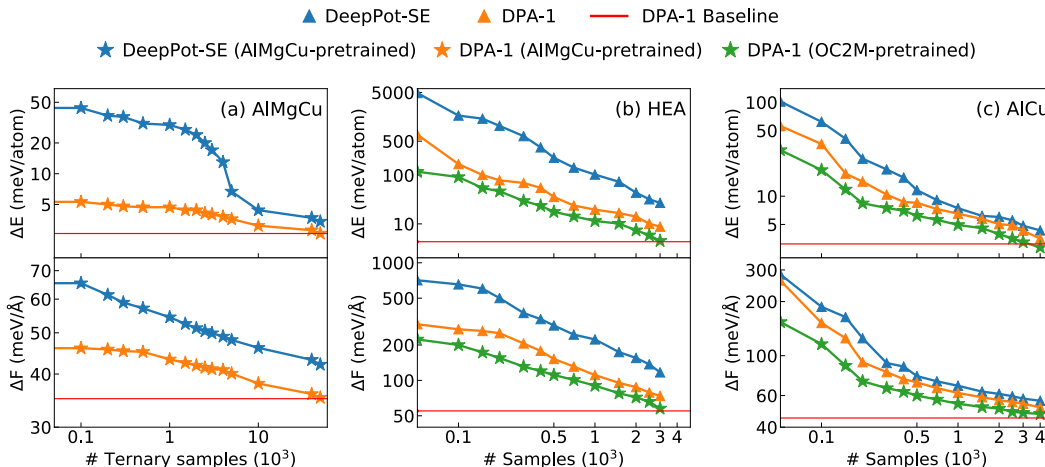


Figure 2: Learning curves of both energy and force with DeepPot-SE and DPA-1, under different setups and on different systems. (a) Learning curves on the AlMgCu ternary subset, with DeepPot-SE and DPA-1 models pretrained on single-element and binary subsets; (b-c) Learning curves on HEA (b) and AlCu (c), with DeepPot-SE (from scratch) and DPA-1 (both from scratch and pretrained on OC2M). Red line represents the full-data-training baseline with DPA-1.

We started with a relatively simple task to compare DeepPot-SE and DPA-1. In this task, both the two models were pretrained using single-element and binary subsets of the AlMgCu systems, and the learning curves were obtained using the AlMgCu ternary subset. As shown in Fig. 2(a), DPA-1 exhibits a much better sample efficiency than DeepPot-SE, which should be expected.

Next, we used the OC2M dataset, which contains 56 elements, to pretrain DPA-1 and evaluated its performance on the HEA systems and the AlCu systems (Figs. 2(b) and (c), respectively). As shown in Fig. 3(c), the training cost of DeepPot-SE scales quadratically with the number of elements, making its pretraining computationally infeasible, while the number of elements has no effects on the training cost of DPA-1. It is observed that the sample efficiency of DPA-1 pretrained on OC2M is generally better than DPA-1 from scratch, while DeepPot-SE from scratch is the worst. Moreover, compared with AlCu systems, the improvement of pretraining is much more significant for HEA systems, possibly due to the fact that the number of elements of HEA is much larger than AlCu, and the local chemical environment is much more complicated.

We notice that several methods, such as Gemnet [11] etc, have produced similar models on OC2M dataset, while the corresponding models have billions of parameters and the training procedure usually needs thousands of GPU hours to converge. DPA-1 only takes less than 200 GPU hours for training with less than one million parameters and achieves decent results (energy MAE 0.681 vs 0.286 eV for DPA-1 and Gemnet-OC [34]). DPA-1 is also quite efficient for molecular dynamics studies, which will be left to future works.

### 3.4 Interpretability of type embedding learned from pretraining

To see whether DPA-1 can learn physically meaningful information from pretraining, we investigated the 3-dimensional principal component analysis (PCA) visualization of the learned type embeddings in the OC2M-pretrained model. Interestingly, as shown in Fig. 3(a), the arrangement of the elements generally follows the shape of a downward spiral. Elements belonging to the same period are lined up in the direction of the spiral; while elements belonging to the same family are listed in the direction orthogonal to the spiral. Even though some transition metal elements are almost bounded together, this rule still roughly holds. It is observed that C, N and O are outliers, possibly because in OC2M, C, N and O are mostly in organic molecules, which serve as adsorbates and have chemical environments that are very different from other elements.

In addition, we performed interpolation experiments for the type embedding of Li, an element unseen in OC2M. As shown in Fig. 3(b), we let  $T_{Li} = \lambda(Na) * T_{Na} + (1 - \lambda(Na)) * T_H$ , since Li lies between H and Na in the same family. When tested on the SSE system, only the bias in the atomic



energy is changed, since the setup of the electronic method used to label the SSE system is different from that for OC2M, which typically causes an energy shift. It is found that the RMSE of energy and force shows a sudden drop when  $\lambda(Na) = 0.7$ , which meets the chemical intuition and further confirms the interpretability of the pretrained DPA-1 model.

## 4 Summary

In this paper, we developed DPA-1, an attention-based Deep Potential model that allows for large-scale pretraining on atomistic datasets. We tested DPA-1 from different aspects, showing its excellent performance in terms of its accuracy on various datasets when trained from scratch, as well as its sample efficiency when pretrained with existing data. Further investigations on the type embedding parameters suggests the interpretability of DPA-1 pretrained on OC2M.

In the future, it will be of interest to extend the training dataset to cover the full periodic table, and, in particular, see a more converged “spiral” in the latent space; the embedding information of local chemical environments may be useful to characterize different conformations. Multi-task and unsupervised training schemes would worth exploring; and, for downstream tasks, just like what has happened in the fields of CV and NLP, schemes like model compression, distillation, and transfer, etc., are desperately needed. We leave these possibilities and more applications to future works.

## 5 Acknowledgements

The work of H.W. was supported by the National Science Foundation of China under Grant No.11871110 and 12122103. We thank Y.L., Z.L. and G.K. for inspiring discussions. The computational resource was supported by the Bohrium Cloud Platform at DP technology.

## References

- [1] Jörg Behler and Michele Parrinello. Generalized neural-network representation of high-dimensional potential-energy surfaces. *Physical review letters*, 98(14):146401, 2007.
- [2] Albert P Bartók, Mike C Payne, Risi Kondor, and Gábor Csányi. Gaussian approximation potentials: The accuracy of quantum mechanics, without the electrons. *Physical review letters*, 104(13):136403, 2010.
- [3] Aidan P Thompson, Laura P Swiler, Christian R Trott, Stephen M Foiles, and Garritt J Tucker. Spectral neighbor analysis method for automated generation of quantum-accurate interatomic potentials. *Journal of Computational Physics*, 285:316–330, 2015.
- [4] Justin Gilmer, Samuel S Schoenholz, Patrick F Riley, Oriol Vinyals, and George E Dahl. Neural message passing for quantum chemistry. In *International conference on machine learning*, pages 1263–1272. PMLR, 2017.
- [5] Kristof Schütt, Pieter-Jan Kindermans, Huziel Enoc Sauceda Felix, Stefan Chmiela, Alexandre Tkatchenko, and Klaus-Robert Müller. Schnet: A continuous-filter convolutional neural network for modeling quantum interactions. *Advances in neural information processing systems*, 30, 2017.
- [6] Linfeng Zhang, Jiequn Han, Han Wang, Roberto Car, and EJPRL Weinan. Deep potential molecular dynamics: a scalable model with the accuracy of quantum mechanics. *Physical review letters*, 120(14):143001, 2018.
- [7] Linfeng Zhang, Jiequn Han, Han Wang, Wissam Saidi, Roberto Car, et al. End-to-end symmetry preserving inter-atomic potential energy model for finite and extended systems. *Advances in Neural Information Processing Systems*, 31, 2018.
- [8] Ralf Drautz. Atomic cluster expansion for accurate and transferable interatomic potentials. *Physical Review B*, 99(1):014104, 2019.
- [9] Johannes Gasteiger, Janek Groß, and Stephan Günnemann. Directional message passing for molecular graphs. In *International Conference on Learning Representations*, 2019.

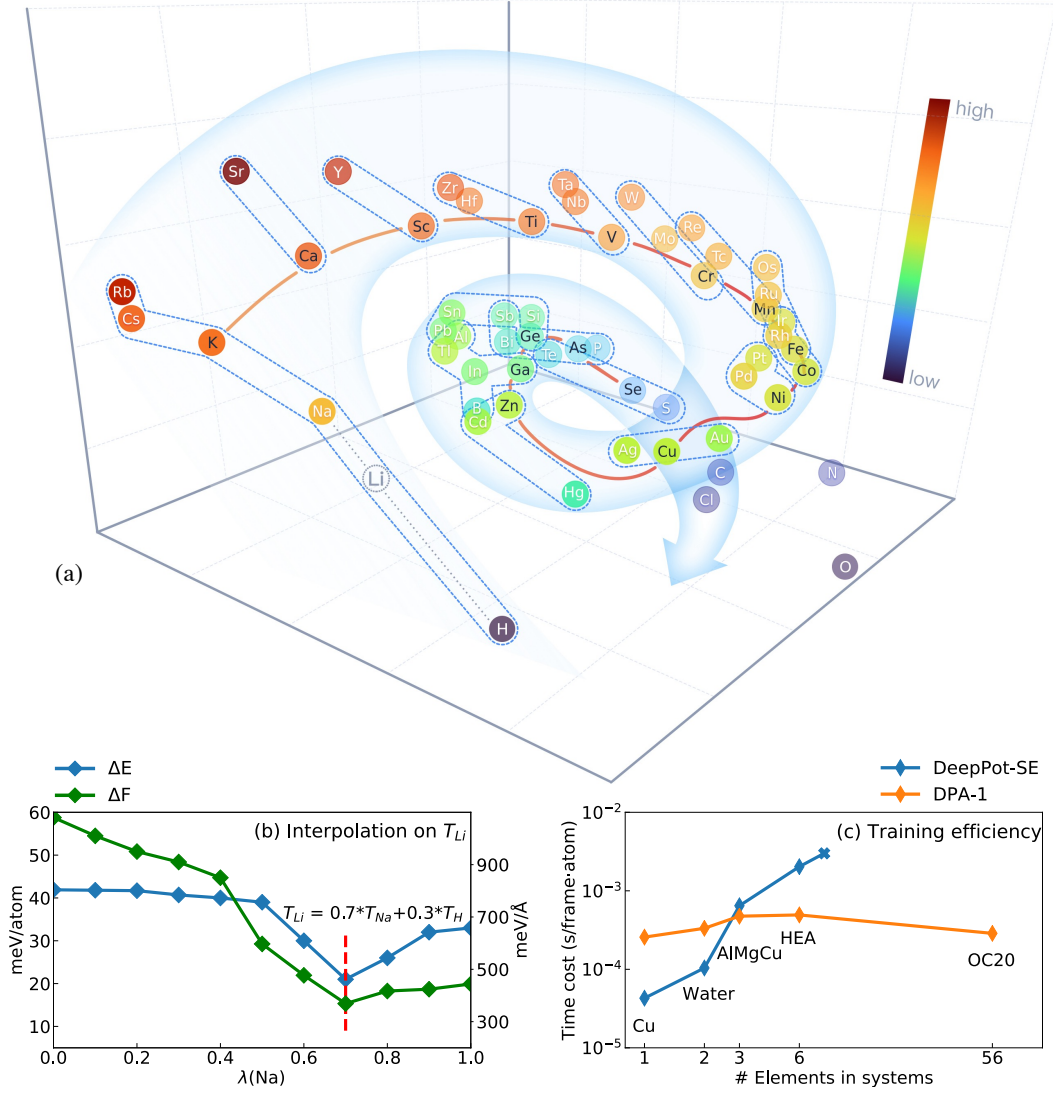


Figure 3: (a) 3-dimensional PCA visualization of the learned type embeddings of DPA-1 pretrained on OC2M. These 56 elements are roughly arranged on a *spiral* in the latent space. Elements in the fourth period are connected with the red line and elements belonging to the same family are grouped by the blue dot lines. Colors on the names of the elements represent the height in  $z$ -axis. We use dashed circle to denote the hypothetical position of Li, which is not contained in OC2M. See text for discussions. (b) RMSE of energy and force for SSE systems given by DPA-1 pretrained on OC2M, as functions of linear interpolation coefficient  $\lambda(Na)$ . Since Li is not contained in OC2M, we let  $T_{Li} = \lambda(Na) * T_{Na} + (1 - \lambda(Na)) * T_H$  be the interpolated type embedding of Li. The OC2M-pretrained model with this interpolation and modified energy bias is directly tested on SSE systems without further training. (c) Training efficiency of DPA-1 and DeepPot-SE (considering type information of both two sides) with the growing number of element types in training systems. The maximum number of neighboring atoms to be considered is set to 120 in all the experiments.

- [10] Yaolong Zhang, Ce Hu, and Bin Jiang. Embedded atom neural network potentials: Efficient and accurate machine learning with a physically inspired representation. *The journal of physical chemistry letters*, 10(17):4962–4967, 2019.
- [11] Johannes Gasteiger, Florian Becker, and Stephan Günnemann. Gemnet: Universal directional graph neural networks for molecules. *Advances in Neural Information Processing Systems*, 34:6790–6802, 2021.
- [12] Volker L Deringer, Albert P Bartók, Noam Bernstein, David M Wilkins, Michele Ceriotti, and Gábor Csányi. Gaussian process regression for materials and molecules. *Chemical Reviews*, 121(16):10073–10141, 2021.
- [13] Oliver T Unke, Stefan Chmiela, Huziel E Sauceda, Michael Gastegger, Igor Poltavsky, Kristof T Schütt, Alexandre Tkatchenko, and Klaus-Robert Müller. Machine learning force fields. *Chemical Reviews*, 121(16):10142–10186, 2021.
- [14] Tongqi Wen, Linfeng Zhang, Han Wang, Weinan E, and David J Srolovitz. Deep potentials for materials science. *Materials Futures*, 2022.
- [15] Albert P. Bartók, James Kermode, Noam Bernstein, and Gábor Csányi. Machine learning a general-purpose interatomic potential for silicon. *Phys. Rev. X*, 8:041048, Dec 2018.
- [16] Volker L Deringer, Miguel A Caro, and Gábor Csányi. A general-purpose machine-learning force field for bulk and nanostructured phosphorus. *Nature communications*, 11(1):1–11, 2020.
- [17] Linfeng Zhang, Han Wang, Roberto Car, and Weinan E. Phase diagram of a deep potential water model. *Phys. Rev. Lett.*, 126:236001, Jun 2021.
- [18] Wanrun Jiang, Yuzhi Zhang, Linfeng Zhang, and Han Wang. Accurate deep potential model for the al–cu–mg alloy in the full concentration space. *Chinese Physics B*, 30(5):050706, 2021.
- [19] Wojciech J. Szlachta, Albert P. Bartók, and Gábor Csányi. Accuracy and transferability of gaussian approximation potential models for tungsten. *Phys. Rev. B*, 90:104108, Sep 2014.
- [20] Xiaoyang Wang, Yinan Wang, Linfeng Zhang, Fuzhi Dai, and Han Wang. A tungsten deep neural-network potential for simulating mechanical property degradation under fusion service environment. *Nuclear Fusion*, 2022.
- [21] YiNan Wang, LinFeng Zhang, Ben Xu, XiaoYang Wang, and Han Wang. A generalizable machine learning potential of Ag–Au nanoalloys and its application to surface reconstruction, segregation and diffusion. *Modelling and Simulation in Materials Science and Engineering*, 30(2):025003, dec 2021.
- [22] Tongqi Wen, Rui Wang, Linyu Zhu, Linfeng Zhang, Han Wang, David J. Srolovitz, and Zhaoxuan Wu. Specialising neural network potentials for accurate properties and application to the mechanical response of titanium. *npj computational materials*, 7:206, 2021.
- [23] Evgeny V Podryabinkin and Alexander V Shapeev. Active learning of linearly parametrized interatomic potentials. *Computational Materials Science*, 140:171–180, 2017.
- [24] Justin S Smith, Ben Nebgen, Nicholas Lubbers, Olexandr Isayev, and Adrian E Roitberg. Less is more: Sampling chemical space with active learning. *The Journal of chemical physics*, 148(24):241733, 2018.
- [25] Linfeng Zhang, De-Ye Lin, Han Wang, Roberto Car, and E Weinan. Active learning of uniformly accurate interatomic potentials for materials simulation. *Physical Review Materials*, 3(2):023804, 2019.
- [26] Yuzhi Zhang, Haidi Wang, Weijie Chen, Jinzhe Zeng, Linfeng Zhang, Han Wang, and E Weinan. Dp-gen: A concurrent learning platform for the generation of reliable deep learning based potential energy models. *Computer Physics Communications*, 253:107206, 2020.
- [27] Walter Kohn and Lu Jeu Sham. Self-consistent equations including exchange and correlation effects. *Physical review*, 140(4A):A1133, 1965.

- [28] Richard Car and Mark Parrinello. Unified approach for molecular dynamics and density-functional theory. *Physical review letters*, 55(22):2471, 1985.
- [29] Olga Russakovsky, Jia Deng, Hao Su, Jonathan Krause, Sanjeev Satheesh, Sean Ma, Zhiheng Huang, Andrej Karpathy, Aditya Khosla, Michael Bernstein, et al. Imagenet large scale visual recognition challenge. *International journal of computer vision*, 115(3):211–252, 2015.
- [30] Alexey Dosovitskiy, Lucas Beyer, Alexander Kolesnikov, Dirk Weissenborn, Xiaohua Zhai, Thomas Unterthiner, Mostafa Dehghani, Matthias Minderer, Georg Heigold, Sylvain Gelly, et al. An image is worth 16x16 words: Transformers for image recognition at scale. *arXiv preprint arXiv:2010.11929*, 2020.
- [31] Jacob Devlin, Ming-Wei Chang, Kenton Lee, and Kristina Toutanova. Bert: Pre-training of deep bidirectional transformers for language understanding. *arXiv preprint arXiv:1810.04805*, 2018.
- [32] Tom Brown, Benjamin Mann, Nick Ryder, Melanie Subbiah, Jared D Kaplan, Prafulla Dhariwal, Arvind Neelakantan, Pranav Shyam, Girish Sastry, Amanda Askell, et al. Language models are few-shot learners. *Advances in neural information processing systems*, 33:1877–1901, 2020.
- [33] Chi Chen and Shyue Ping Ong. A universal graph deep learning interatomic potential for the periodic table. *arXiv preprint arXiv:2202.02450*, 2022.
- [34] Johannes Gasteiger, Muhammed Shuaibi, Anuroop Sriram, Stephan Günnemann, Zachary Ulissi, C Lawrence Zitnick, and Abhishek Das. How do graph networks generalize to large and diverse molecular systems? *arXiv preprint arXiv:2204.02782*, 2022.
- [35] Ashish Vaswani, Noam Shazeer, Niki Parmar, Jakob Uszkoreit, Llion Jones, Aidan N Gomez, Łukasz Kaiser, and Illia Polosukhin. Attention is all you need. *Advances in neural information processing systems*, 30, 2017.
- [36] Lowik Chanussot, Abhishek Das, Siddharth Goyal, Thibaut Lavril, Muhammed Shuaibi, Morgane Riviere, Kevin Tran, Javier Heras-Domingo, Caleb Ho, Weihua Hu, et al. Open catalyst 2020 (oc20) dataset and community challenges. *ACS Catalysis*, 11(10):6059–6072, 2021.
- [37] Justin S Smith, Olexandr Isayev, and Adrian E Roitberg. Ani-1: an extensible neural network potential with dft accuracy at force field computational cost. *Chemical science*, 8(4):3192–3203, 2017.
- [38] Justin S Smith, Benjamin T Nebgen, Roman Zubatyuk, Nicholas Lubbers, Christian Devereux, Kipton Barros, Sergei Tretiak, Olexandr Isayev, and Adrian E Roitberg. Approaching coupled cluster accuracy with a general-purpose neural network potential through transfer learning. *Nature communications*, 10(1):1–8, 2019.
- [39] Shengchao Liu, Hanchen Wang, Weiyang Liu, Joan Lasenby, Hongyu Guo, and Jian Tang. Pre-training molecular graph representation with 3d geometry. In *International Conference on Learning Representations*, 2022.
- [40] Hannes Stärk, Dominique Beaini, Gabriele Corso, Prudencio Tossou, Christian Dallago, Stephan Günnemann, and Pietro Liò. 3d infomax improves gnns for molecular property prediction. *arXiv preprint arXiv:2110.04126*, 2021.
- [41] Gengmo Zhou, Zhifeng Gao, Qiankun Ding, Hang Zheng, Hongteng Xu, Zhewei Wei, Linfeng Zhang, and Guolin Ke. Uni-mol: A universal 3d molecular representation learning framework. 2022.
- [42] Meng-Hao Guo, Tian-Xing Xu, Jiang-Jiang Liu, Zheng-Ning Liu, Peng-Tao Jiang, Tai-Jiang Mu, Song-Hai Zhang, Ralph R Martin, Ming-Ming Cheng, and Shi-Min Hu. Attention mechanisms in computer vision: A survey. *Computational Visual Media*, pages 1–38, 2022.
- [43] Andrea Galassi, Marco Lippi, and Paolo Torroni. Attention in natural language processing. *IEEE Transactions on Neural Networks and Learning Systems*, 32(10):4291–4308, 2020.

- [44] Diederik P Kingma and Jimmy Ba. Adam: A method for stochastic optimization. *arXiv preprint arXiv:1412.6980*, 2014.
- [45] Jianxing Huang, Linfeng Zhang, Han Wang, Jinbao Zhao, Jun Cheng, and Weinan E. Deep potential generation scheme and simulation protocol for the li10gep2s12-type superionic conductors. *The Journal of Chemical Physics*, 154(9):094703, 2021.
- [46] Anubhav Jain, Shyue Ping Ong, Geoffroy Hautier, Wei Chen, William Davidson Richards, Stephen Dacek, Shreyas Cholia, Dan Gunter, David Skinner, Gerbrand Ceder, et al. Commentary: The materials project: A materials genome approach to accelerating materials innovation. *APL materials*, 1(1):011002, 2013.
- [47] Stefan Chmiela, Alexandre Tkatchenko, Huziel E Sauceda, Igor Poltavsky, Kristof T Schütt, and Klaus-Robert Müller. Machine learning of accurate energy-conserving molecular force fields. *Science advances*, 3(5):e1603015, 2017.
- [48] Raghunathan Ramakrishnan, Pavlo O Dral, Matthias Rupp, and O Anatole Von Lilienfeld. Quantum chemistry structures and properties of 134 kilo molecules. *Scientific data*, 1(1):1–7, 2014.

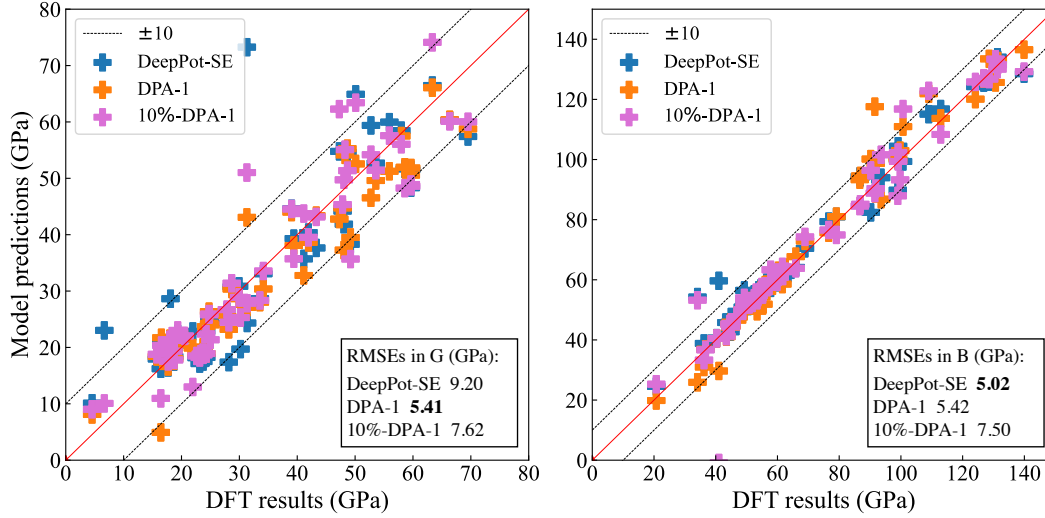


Figure A.1: Test of trained DeepPot-SE and DPA-1 models on shear (a) and bulk (b) moduli of AlMgCu systems. Both DeepPot-SE and DPA-1 models are trained on all subsets of AlMgCu systems, while 10%-DPA-1 model used less ternary samples (10%).

## A Test on elastic moduli

Test results of elastic moduli of AlMgCu systems are shown in Fig. A.1, with the overall RMSE of both moduli are respectively 7.41, **5.41** and 7.56 GPa for DeepPot-SE, DPA-1 and 10%-DPA-1. Finite difference method is used to calculate the elastic moduli, where the maximum norm and shear deformation with respect to the equilibrium conformation are both 2%.

## B Hyperparameters in sample efficiency tests

To generate the learning curves of sample efficiency in Sec. 3.3, we started from 50 randomly selected samples and set the training steps to be 10w during each iteration. The probabilities to visit the historical and newly added samples are set to 0.9 and 0.1, respectively.

## C Code availability

The codes of DPA-1 are in the repository of DeePMD-kit: <https://github.com/deepmodeling/deepmd-kit>. All the experiments are performed on single Nvidia® Tesla V100.